JCTC Journal of Chemical Theory and Computation

ARTICLE

pubs.acs.org/JCTC

Robust and Efficient Constrained DFT Molecular Dynamics Approach for Biochemical Modeling

Jan Řezáč,[†] Bernard Lévy,[‡] Isabelle Demachy,[‡] and Aurélien de la Lande*[,‡]

[†]Institute of Organic Chemistry and Biochemistry, Academy of Sciences of the Czech Republic and Center for Biomolecules and Complex Molecular Systems, Flemingovo nam. 2, 166 10 Prague 6, Czech Republic

[‡]Laboratoire de Chimie Physique, CNRS UMR 8000, Université Paris-Sud. Bât. 349, Campus d'Orsay, 15 rue Jean Perrin, 91405 Orsay Cedex, France

ABSTRACT: Constrained density functional theory (cDFT) is a powerful tool to investigate the dynamics of the electrons accompanying various physical−chemical processes. In this article we present our recent progresses in the implementation of the method in the parallelized version of the DFT program deMon2k. We take advantage of the possibility to express atomic densities in terms of linear combination of Hermite Gaussian functions to improve the computation of the cDFT integration weights within the Hirshfeld and Voronoi deformation density electronic population approaches. The efficiency of the method is illustrated on the computation of the average electronic coupling for an electron transfer (ET) through a glycine polypeptide of increasing length. The sampling is based on cDFT and hybrid cDFT/molecular mechanics molecular dynamics simulations. We also report the first estimations of quantum decoherence times from cDFT-based simulations for an ET reaction.

INTRODUCTION

Constrained density functional theory (cDFT) is a modern theoretical approach enabling the investigation of the electronic dynamical aspects of many physicochemical processes, like charge-transfer reactions and singlet fission or singlet triplet transitions to name but a few examples. Although cDFT has a long history, starting with the work of Dederichs et al.[1] in the 1980's and Hong et al.[2,3] in the 1990′s, it has regained attention in the last years thanks to the novel framework proposed by Wu and Van Voorhis.[4,5] This latter approach is rooted on the optimized effective potential theory.[6] The underlying idea of cDFT is to constraint a partial charge (or spin) of a group of atoms (thereafter referred as A) to an arbitrary value while minimizing the DFT energy functional. The constrained quantity is defined as an integral of the density (or spin density) over the selected atoms. A Lagrange multiplier technique is used to optimize a constraining potential along with the self consistent field (SCF) procedure in order to fulfill the desired charge or spin constraint (N_{cns}). In cDFT the functional F to minimize is thus:

$$F[\rho] \equiv E[\rho] + \lambda_{cns} \sum_{\sigma=\alpha,\beta} \left(\int \rho_\sigma(r) w(r) \mathrm{d}r - N_{cns} \right) \quad (1)$$

where $E[\rho]$ is the usual DFT functional, σ is the electronic spin, and $w(r)$ a weighting function that ensures that the integration of the electronic density over the space is restricted to domain A. Note that A may comprise one or more atoms. Different technical prescriptions have been reported using the linear combination of atomic orbitals (LCAO) Kohn−Sham (KS) framework with either localized atomic orbitals[4,7] or plane wave basis sets.[8] We also mention the promising extensions of cDFT to the tight binding DFT[9] or the linear scaling DFT[10] approaches that have been recently reported. Such promising developments open the door toward application of cDFT to larger space and time scales.

Our long-term objective is to develop a set of accurate computational tools based on the cDFT technique to investigate fine quantum mechanical processes, such as charge or hydrogen transfers occurring in the biological medium. In a previous paper we have presented a basic implementation of the method in the DFT program deMon2k.[11] In deMon2k[12] the LCAO-KS cDFT computations are performed in the context of the auxiliary DFT (ADFT) formalism meaning that an auxiliary fitted density $\tilde{\rho}$ is used to compute both the coulomb and the exchange−correlation potentials and energies (eq 2, in case of a closed-shell system).[13,14]

$$\begin{aligned} F[\rho] = & \sum_{p,q} P_{pq} H^{core}_{pq} \\ & + \sum_{p,q} \sum_{k} P_{pq} x_k \langle pq||k\rangle - \frac{1}{2} \sum_{k,l} x_l x_k \langle k||l\rangle \\ & + E_{XC}[\tilde{\rho}] + \lambda_{cns}\left(\left[\sum_{pq} P_{pq} W_{pq} - N_{cns} \right] \right) \end{aligned} \quad (2)$$

In this equation P is the electronic density matrix, H^{core} is the core Hamiltonian containing the electronic kinetic energy and the electron−nuclei attraction potentials, W is the so-called weight matrix that defines which regions of real space are to subjected to charge constraint, p and q represent Gaussian-type atomic orbitals, while k and l represent the Hermite Gaussian-type basis functions used to expand the auxiliary electronic density by

$$\tilde{\rho}(r) = \sum_{k} x_k k(r) \quad (3)$$

Received: August 16, 2011
Published: December 16, 2011

So far our cDFT implementation has been applied to derive parameters for interpretative models of biological long-range electron transfers (ETs)[11] or to investigate transitions between distinct topologies of the electron localization function.[15] Despite these first applications, the implementation was not efficient enough to enable the modeling of large systems at the cDFT level or to perform Born−Oppenheimer molecular dynamics (BOMD) simulations. Here we present the extensions that we have brought recently in order to make the technique suitable for hybrid cDFT/MD simulations in deMon2k. In the first section, we detail the mathematical background of cDFT as implemented in deMon2k to compute the constrained DFT energy and its derivatives with respect to the nuclear coordinates. A particular emphasis is put on the influence of the population schemes on the cDFT results taking an organic mixed-valence compound as a test case. The hybrid cDFT/MM scheme is then tested by investigating the decay of the average electronic coupling for the long-range ET between two lithium atoms through a polypeptide of increasing length. We also show how characteristic decoherence times [i.e., the decay of the Franck−Condon (FC) overlap in the present framework] can be estimated from constrained DFT BOMD.

CONSTRAINED DFT IN DEMON2K

As introduced before the objective cDFT is to enforce the charge of the spin density of a group of atoms in the DFT computation. By construction, the cDFT approach requires choosing a population scheme to define the atomic charges within the molecules of interest. It is well known that since the charge of an atom is not uniquely defined in quantum mechanics some arbitrariness is introduced at this point. A wide range of methods can be used in deMon2k for population analysis and cDFT computations. These are the Mulliken, Löwdin, Becke, Voronoi, Becke/Voronoi deformation density[16] (BDD/VDD), and Hirshfeld[17] population schemes. The following expressions are used to calculate the atomic charges, taking the example of atom A:

$$Q_A^{\text{Mulliken}} = Z_A - \sum_{\mu \in A} (PS)_{\mu\mu} \tag{4}$$

$$Q_A^{\text{Löwdin}} = Z_A - \sum_{\mu \in A} (S^{1/2}PS^{1/2})_{\mu\mu} \tag{5}$$

$$Q_A^{\text{Becke}} = Z_A - \int_{\text{Becke cell of A}} \rho(r)\mathrm{d}r \tag{6}$$

$$Q_A^{\text{Voronoi}} = Z_A - \int_{\text{Voronoi cell of A}} \rho(r)\mathrm{d}r \tag{6'}$$

$$Q_A^{\text{Hirshfeld}} = Z_A - \int \rho(r)\frac{\rho_A^a(r)}{\rho^{\text{promolecule}}(r)}\mathrm{d}r \tag{7}$$

$$Q_A^{\text{BDD}} = \int_{\text{Becke cell of A}} [\rho(r) - \rho^{\text{promolecule}}(r)]\mathrm{d}r \tag{8}$$

$$Q_A^{\text{VDD}} = \int_{\text{Voronoi cell of A}} [\rho(r) - \rho^{\text{promolecule}}(r)]\mathrm{d}r \tag{8'}$$

$$\rho^{\text{promolecule}}(r) = \sum_{\text{all atoms } j} \rho_j^a(r) \tag{9}$$

In the above expressions Z_A is the nuclear charge of atom A, S is the overlap matrix of the atomic orbitals, and ρ_j^a are the atomic densities of the isolated atoms. The superposition of the atomic densities gives rise to the so-called promolecular density. Some of the above expressions involve integration over Voronoi or Becke cells. The Voronoi cell of an atom, for example A, is defined as the ensemble of space points that is closer to atom A than from any other atom. The Becke cell of atom A is constructed similarly except that a smoothing function is applied at the borders between adjacent cells. As a consequence, the Becke cells overlap one with each other, hence their qualification as fuzzy. The integration of the electron density over the Becke or the Voronoi cell gives access to the number of electrons of the atom and to its charge. Because the smoothing functions decay rapidly from one to zero at the borders between cells, the Becke and Voronoi schemes usually render very similar charges. In the remainder of the paper, we will only consider the Becke scheme. The above approach consisting of integrating the relaxed electronic density over the Voronoi or the Becke cells should not be confused with the VDD/BDD approach. Within the VDD (or BDD) approach the charges are calculated by integration of the difference between the relaxed electronic density of the molecule and the promolecular density over the Voronoi (or Becke) cell. Again the VDD charges are usually found to be very close to the BDD charges.

Within the LCAO framework used in deMon2k, the electron density associated to the group of atoms A is computed according to

$$\int \rho(r)w(r)\mathrm{d}r = \sum_{pq} P_{pq}W_{pq} = Tr(PW) \tag{10}$$

W can be seen as a sparse overlap matrix of the atomic orbitals. Its precise elements are computed differently depending on the population scheme chosen to perform the cDFT computation.[8,18] In this paper we mainly describe the Hirshfeld population scheme since it is the one we mostly developed in the ADFT context. When using the Hirshfeld approach the weight matrix elements are computed numerically on the DFT integration grid. This operation is done only once at the beginning of the SCF computation:

$$W_{pq} = \sum_i a_i \varphi_p(r_i)\varphi_q(r_i)w_i \tag{11}$$

The terms a_i are the integration weights which are computed in deMon2k according to the Gauss−Chebyshev quadrature scheme coupled to the partition of the real space into atomic fuzzy Becke cells.[19−21] The terms w_i specify the contribution of each grid point to the electron density associated to the group of atoms whose charge has to be constrained. In the Hirshfeld approach the w_i are computed using the electronic densities of the isolated atoms $\rho^a(r)$:[17]

$$w_i = \frac{\sum_{\text{atoms in A}} \rho^a(r_i)}{\sum_{\text{all atoms}} \rho^a(r_i)} \tag{12}$$

This expression takes into account the chemical nature of the atoms on the basis of the electronic density they would have if they could be isolated from the rest of the molecule. This provides valuable advantage over partitioning methods that are strictly based on geometrical considerations, like the Becke charges. Equations 11 and 12 enable computing the constraining term entering eq 1. The procedure used in

deMon2k to optimize the Lagrange multiplier has been detailed in ref 11.

ENERGY GRADIENTS

To perform geometry optimizations or MD simulations, one also needs the contributions of the constraint energy term to the gradients. From eq 2 one straightforwardly gets the derivatives of the constraining energy with respect to the nuclear degree of freedom X as

$$\frac{\partial E_{\mathrm{cns}}}{\partial X} = \lambda_{\mathrm{cns}} \sum_{pq}\sum_{i} \frac{\partial P_{pq} a_i w_i \varphi_p(r_i)\varphi_q(r_i)}{\partial X} \tag{13}$$

$$\begin{aligned}\frac{\partial E_{\mathrm{cns}}}{\partial X} = \lambda_{\mathrm{cns}} \sum_{pq}\sum_{i} \Bigg[& \frac{\partial P_{pq}}{\partial X} a_i w_i \varphi_p(r_i)\varphi_q(r_i) \\ & + \frac{\partial a_i}{\partial X} P_{pq} w_i \varphi_p(r_i)\varphi_q(r_i) + \frac{\partial w_i}{\partial X} P_{pq} a_i \varphi_p(r_i)\varphi_q(r_i) \\ & + 2\frac{\partial \varphi_p(r_i)}{\partial X} P_{pq} w_i \varphi_q(r_i)\Bigg]\end{aligned} \tag{14}$$

As for the other energy terms derivatives in deMon2k, the explicit derivatives of the density matrix elements can be eliminated using the Pulay relationship.[22] In addition it has been shown that if the DFT integration grid used for the energy computation is of sufficiently good quality, it is safe to neglect the terms involving the derivatives of the integration weights a_i.[23] Consequently the energy derivative expression reduces to

$$\frac{\partial E_{\mathrm{cns}}}{\partial X} = \lambda_{\mathrm{cns}} \sum_{pq}\sum_{i} \left[\frac{\partial w_i}{\partial X} P_{pq} a_i \varphi_p(r_i)\varphi_q(r_i) + 2\frac{\partial \varphi_p(r_i)}{\partial X} \varphi_q(r_i) P_{pq} a_i w_i \right] \tag{15}$$

given that[8]

$$\frac{\partial w_i}{\partial X} = -\frac{1}{\sum_j \rho_j(r_i)} \frac{\partial \rho_a(r_i)}{\partial X} G_i^X \tag{16}$$

$$G_i^X = w_i \tag{17}$$

if X does not belong to A, and

$$G_i^X = w_i - 1 \tag{18}$$

if X belongs to A.

The comparison of the gradient components computed analytically with eq 15 to the numerical counterparts including all the terms of eq 14 for various test case molecules showed that the approximations leading to eq 15 are acceptable.

PRACTICAL DEFINITION OF THE ATOMIC DENSITIES

We now describe the mathematical form of the atomic densities $\rho^a(r)$ needed to calculate the Hirshfeld integration weights by eq 12. In a paper describing a plane-wave implementation of cDFT, Oberhofer et al. proposed to use Slater or Gaussian functions.[8] In the case of a Gaussian expression one can use

$$\rho^a_{\mathrm{Gauss}}(r) = \frac{N_a^{\mathrm{el}}}{\sqrt{2\pi}\sigma_a} \mathrm{e}^{-(Ra - r)^2/2\sigma_a^2} \tag{19}$$

With N_a^{el} the number of electrons of the neutral atom and σ_a the width of the Gaussian centered at Ra. The latter parameter characterizes the spread of the atomic electronic density. A drawback of this type of expression is the arbitrariness in the choice of σ_a. One could take, for example, the covalent radii of the atom or a fraction of it. In their study of the self-exchange reaction between aqueous $Ru^{2+/3+}$ complexes, Oberhofer et al., for example, proposed to assign a value of 0.6 Å for hydrogen or oxygen atoms and a value of 1.0 Å for ruthenium atoms.[8] A more realistic representation than eq 19 would be to use atomic densities ρ^a determined by ab initio methods. The possibility exploited in such a case is to save the atomic density matrices obtained in a preliminary atomic DFT computation. To take advantage of the ADFT implementation in deMon2k, we have chosen to use the alternative of expressing $\tilde{\rho}^a(r)$ as a linear combination of Hermite Gaussian functions $k(r)$.

$$\tilde{\rho}^a_{\mathrm{DFT}}(r) = \sum_k x_k k(r) \tag{20}$$

$$k(r) = \lambda_{k_x}(x_{\mathrm{A}})\lambda_{k_y}(y_{\mathrm{A}})\lambda_{k_z}(z_{\mathrm{A}})\mathrm{e}^{-\xi_k(r - R_{\mathrm{A}})^2} \tag{21}$$

$$\lambda_{k_x}(x_{\mathrm{A}}) = \xi_k^{k_x/2} H_{k_x}(\xi_k^{k_x/2} x_{\mathrm{A}}) \tag{22}$$

where H_{k_x} denotes a Hermite polynomial of order k_x. The parameters ξ_k are the expansion coefficients. The tilde is used to denote an electronic density expanded on auxiliary basis functions. Although apparently complex, this representation is a natural choice for our implementation since deMon2k already makes intensive use of such expansions of the electronic density in the context of the ADFT framework.[24] The auxiliary basis functions k are automatically generated by the program or stored in an external library; the only unknown quantities being the coefficients x_k. To determine them, atomic DFT computations are carried out before the main cDFT computation, and the coefficients x_k are adjusted so as to reproduce the coulomb potential created by the orbital electronic density ρ^a. A detailed description of the variational fitting procedure can be found in ref 13. The resulting coefficients x_k are kept in memory and subsequently used in the cDFT computation to calculate the weights w_i. We mention that the time spent in the fitting procedure of the atomic densities is negligible compared to the cDFT computation cost. Moreover, like the core Hamiltonian, the weight matrix has anyway to be computed only once at the beginning of the SCF procedure.

The shapes of the atomic electronic densities of two carbon atoms separated by 1.5 Å obtained with eqs 14 are illustrated in Figure 1 by dashed lines. The orbital DFT density (full lines) serves as the reference. As expected, the auxiliary density closely reproduces the orbital density. It is indeed difficult to differentiate the two curves in such a plot. On the other hand, the Gaussian densities (dashed−dotted lines) strongly differ from the DFT ones in the neighborhood of the carbon nuclei, the latter are

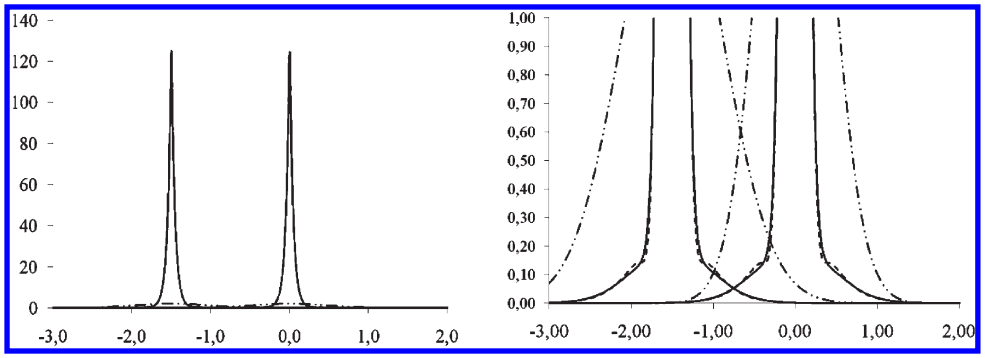

Figure 1. Comparison of the atomic densities of two carbon atoms separated by 1.5 Å. The full and dashed lines are, respectively, the orbital and auxiliary DFT densities. The dashed−dotted line is the 0.4 Å width Gaussian densities. The *x*-axis is the position of the carbon atoms (in Å), while the *y*-axis gives the electronic density (in $Å^{-3}$).

found to be significantly peaked. In view of these results, on a simple case one would probably expect different Hirshfeld atomic charges when investigating real chemical systems. To go deeper and to test the sensitivity of the mathematical expression for ρ^a on the computed Hirshfeld charges and on the structural characteristics of the cDFT optimized geometries, we have considered the tetrathiafulvalene−diquinone radical anion $[QTTFQ]^-$ depicted in Figure 2. This molecule is a type II mixed-valence compound[25] which is often considered as a good practical test case for cDFT performance.[26,27] The computations have been carried out with the Perdew, Burke, and Ernzerhof (PBE) functional[28] and the double ζ valence and polarization functions, adapted for generalized gradient approximation functional (DZVP-GGA) basis set. The GEN-A2 basis set was used to expand the auxiliary densities for the computation of KS matrix elements and also to express the DFT atomic densities by eq 12. An adaptive grid of high accuracy was used (using TOL = 1.0×10^{-8} in deMon2k input standards).[29] For the cDFT computation we have constrained the charge difference between the right-hand side and left-hand side aromatic compounds.

Table 1 gathers the atomic charges obtained on the cDFT optimized $[Q^0TTFQ^-]^-$ form using various population schemes. All the charges reported in Table 1 are computed on the constrained electronic density using the Hirshfeld approach coupled to the $\tilde{\rho}^a_{DFT}$ atomic densities. We first remark that significant differences are found for each atom when going from one population scheme to another, with the noticeable exception of the Hirshfeld/$\tilde{\rho}^a_{DFT}$ and BDD population schemes that give very similar charges. This latter observation is actually consistent with previous analysis reported by other groups comparing the Hirshfeld and the VDD approaches.[16] Otherwise the charges on a given atom may vary by more than 0.25 (see e.g., the carbon or oxygen atoms) or even change sign (see the sulfur atoms), depending on the population scheme. We note that the form of the atomic densities (ρ^a_{Gauss}or $\tilde{\rho}^a_{DFT}$) used to compute the Hirshfeld integration weights has also a strong impact on the computed charges. If one wishes to stay close to the original definition of the atomic charges proposed by Hirshfeld,[17] the DFT atomic densities should be preferred to the Gaussian expressions for cDFT computations. The total charge of each *Q* cycle is de facto different between the different approaches. However beside all these noticeable differences, it is worth remarking that the charge difference between the two cycles is always almost equal to −1, with the exception of the Mulliken approach.

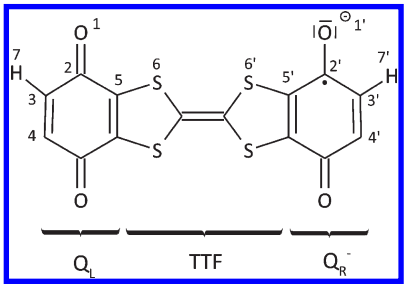

Figure 2. One mesomeric form of the $[QTTFQ]^-$ mixed-valence molecule: the minus charge is localized on the right-hand side cycle (0/-1 electronic state).

We now turn our attention to the effect of the atomic densities on the optimized geometries (Table 2). As expected, the non-constrained DFT optimized structure is geometrically because the −1 charge is delocalized over the two aromatic parts of the molecules. These features do not correspond to the chemistry of this type II mixed-valence molecule.[25] At the opposite the cDFT optimized geometries are in excellent agreement with the optimized geometries of either the fully oxidized or the fully reduced ($[Q_LTTFQ_R]^{0/2-}$) compounds. The Hirshfeld charges computed on the cDFT optimized structures also nicely match those obtained on these reference molecules. The choice of the Gaussian (ρ^a_{Gauss}) or the more faithful DFT ($\tilde{\rho}^a_{DFT}$) atomic densities for the computation of the Hirshfeld integration weights has no strong influence on the optimized structure of $[Q_LTTFQ_R]^-$. Apart from the C−S bond lengths, the two cDFT approaches lead to very similar geometries. In addition both population schemes give similar charge differences between the two cycles despite distinct charge repartitions within the cofactors. We remark nonetheless that the use of the $\tilde{\rho}^a_{DFT}$ atomic densities render atomic charges that are much closer to the mesomeric description of the mixed-valence compound (see, for example, the total charge of each aromatic cycle) than the Gaussian atomic densities. Since the former does not imply any significant increase of the computational cost, we recommend using them in deMon2k cDFT computations.

COMPUTATIONAL EFFICIENCY TESTS

The use of ab initio methods in quantum mechanics (QM) or hybrid QM/molecular mechanics (MM) MD simulations supposes that the computation of the energy and gradients are

Table 1. Partial Atomic Charge on the $[Q_L{}^0TTFQ_R{}^-]^-$ Molecule with Various Population Schemes[a]

	Hirshfeld		BDD	Becke	Mulliken	Löwdin
charge	$\tilde{\rho}^a_{DFT}$	ρ^a_{Gauss}	$\tilde{\rho}^a_{DFT}$			
$q(O_1)/q(O_{1'})$	−0.19/−0.37	−0.38/−0.58	−0.19/−0.39	−0.34/−0.54	−0.24/−0.43	−0.13/−0.33
$q(C_2)/q(C_{2'})$	0.13/0.02	0.18/0.08	0.13/0.04	0.25/0.16	0.31/0.20	0.03/−0.06
$q(C_3)/q(C_{3'})$	−0.02/−0.10	−0.16/−0.24	−0.04/−0.10	0.49/0.43	−0.11/−0.17	−0.06/−0.15
$q(H_7)/q(H_{7'})$	0.07/0.02	0.28/0.24	0.10/0.03	−0.46/−0.52	0.15/0.09	0.13/0.10
$q(C_5)/q(C_{5'})$	0.00/−0.10	0.27/0.18	0.01/−0.10	−0.23/−0.34	−0.19/−0.34	−0.20/−0.31
$q(S_6)/q(S_{6'})$	0.03/0.10	−0.38/−0.30	−0.03/0.07	0.54/0.64	0.17/0.33	0.42/0.53
sum over Q	−0.03/−1.04	0.36/−0.62	0.02/−1.04	−0.58/−1.62	−0.16/−1.3	−0.46/−1.5
Δq	−1.01	−0.98	−1.02	−1.04	−1.14	−1.04

[a] The electronic density on which the charges are calculated results from the convergence of a cDFT run with the Hirshfeld population scheme using the $\tilde{\rho}^a_{DFT}$ atomic densities. The labeling of the atoms is given in Figure 2.

Table 2. Comparison of Regular and Constrained DFT Geometrical Characteristics, Populations Analysis, and Energetics of the QTTQ Molecule in Gas Phase[a]

	optimized geometry				
	DFT			cDFT $[Q_L{}^0TTFQ_R{}^-]^-$	
	$[Q_LTTFQ_R]^0$	$[Q_LTTFQ_R]^{2-}$	$[Q_LTTFQ_R]^-$	$\tilde{\rho}^{DFT}_a$	ρ^{Gauss}_a
			Distances in Å		
$d(O_1-C_2)$	1.244	1.283	1.262	1.242/1.285	1.242/1.284
$d(C_2-C_3)$	1.486	1.454	1.469	1.486/1.453	1.485/1.454
$d(C_3-C_4)$	1.354	1.386	1.368	1.354/1.386	1.353/1.387
$d(C_2-C_5)$	1.476	1.456	1.463	1.478/1.453	1.483/1.449
$d(C_5-S_6)$	1.751	1.769	1.759	1.765/1.755	1.722/1.800
			Populations		
$q(O_1)/q(O_{1'})$	−0.21	−0.36	−0.35	−0.19/−0.37	−0.39/−0.57
$q(C_2)/q(C_{2'})$	0.12	0.03	0.03	0.13/0.02	0.18/0.08
$q(C_3)/q(C_{3'})$	−0.02	−0.10	−0.07	−0.02/−0.10	−0.16/−0.24
$q(H_7)/q(H_{7'})$	0.06	0.02	0.04	0.06/0.02	0.28/0.24
$q(C_5)/q(C_{5'})$	−0.03	−0.06	−0.05	0.00/−0.09	0.28/0.17
sum over Q	−0.16	−0.94	−0.8	−0.04/−1.04	0.38/−0.64
$q(S_6)/q(S_{6'})$	0.12	0.03	0.19	0.03/0.12	−0.39/0.30

[a] The fully reduced molecule was treated as a triplet to ensure a biradical character.

reliable, fast, and numerically stable over the simulation time. The reliability of the cDFT methods to simulation condensed phase ET reactions has already been shown in the past using either other formulations of the method[3] or the one based on the optimized effective potential theory which is used here.[8] Moreover a remarkable strength of the DFT engine in deMon2k is its high speed that is achieved thanks to the use of the most recent auxiliary density techniques[13,24] and efficient parallelization scheme.[30,31] These improvements have, for example, allowed investigations on large systems by means of ab initio Born−Oppenheimer MD simulations.[32−34] On the other hand, the cDFT implementation we employed in our previous studies,[11,15] though numerically correct, was not suitable for hybrid cDFT/MD simulations since it was both too slow and numerically instable (e.g., the SCF process frequently failed to converge even for simple systems). To improve the efficiency of the cDFT calculations, the determination of both the weight matrix, at the beginning of the SCF procedure, and the calculations of energy gradients has been (re)implemented in a more efficient way. Moreover the use of the Hirshfeld scheme now allows taking advantage of the efficient grid integration routines (previously developed for the numerical integration of the XC potential) for the computation of the weight matrix elements and its derivatives. In addition we mention that all the cDFT routines have now been parallelized.

In Table 3 we provide the computational cost for 50 steps of MD simulations in the NVT ensemble using a time step of 0.5 fs for the $[Q_L{}^0TTFQ_R{}^{1-}]^{1-}$ compound. It is apparent from these numbers that cDFT computations do not imply an overall dramatic supplementary cost compared to regular DFT. It is worth remarking that the total time spent to compute the electronic energies for each MD step is similar in DFT and cDFT approaches despite the necessity to optimize the constraining Lagrange multipliers in cDFT. In the course of the simulation each new energy evaluation makes use of the previous electronic density as a guess for the SCF process, therefore the

Table 3. Comparative Computational Costs of DFT and Constrained DFT Born−Oppenheimer MD Simulations[a]

		cDFT	
	DFT	$\tilde{\rho}^{DFT}(r)$	$\rho^{Gauss}(r)$
total cpu, time (s)	2293	3238	3202
first DFT energy, time (s)	229	146	144
all DFT energies, time (s)	1152	1249	1226
avg number of SCF cycles	11.3	6.94	7.10
XC and CNS gradient (s)	144	1330	1325
matrix diag. (no./s)	1571/190	2089/247	2015/248
matrix multip. (no./s)	4840/84	10 336/182	9756/173

[a] The DZVP-GGA basis set and GEN-A2 auxiliary basis set. The computations were run of four processors. The CPU costs for the gradient computation comprise both XC and constraints contributions. For the matrix operations, both the number of operations (no.) and the CPU time in seconds are given.

cDFT remains efficient. Also, as proposed in ref 8, we use an extrapolation of the Lagrange multiplier to provide a guess for each new cDFT computation. As a result, even if the number of matrix multiplications and diagonalization is much larger for cDFT MD, the supplementary time spent to compute the DFT energies remains similar (1152 vs 1250 s). In addition, the cDFT engine does not suffer anymore form SCF instabilities like in our previous implementation. Actually for the case investigated here, the nonconstrained DFT simulation experiences difficulties to optimize the electronic density of the mixed valence state that is a combination of multiple electronic states of similar energies (at least 2). On the contrary, the cDFT approach bypasses this problem by construction so that less SCF cycles are needed to converge the cDFT energies (around 11 vs 7 SCF steps). Although encouraging, these statistics also show that significant efforts should be put in the future on the optimization of the routines of the cDFT energy gradients. A factor of almost 10 is found between the nonconstrained and constrained DFT (144 vs 1330 s). Equations 15−18 operate on the electronic density matrix and the atomic orbital derivatives, thus making the computation of the constraint energy gradients a bottleneck of the overall BOMD simulation. This limitation could be removed in the future by the use of auxiliary density techniques, as this is already done for the XC energy gradients.[13] Such developments are currently under way in our laboratory and will be reported in due course. Nevertheless the present implementation is already found efficient enough to enable dynamical modeling of systems of biological relevance, as we shall show now.

DYNAMICAL ESTIMATIONS OF THE ELECTRONIC COUPLING AND DECAYS OF FC FACTORS

Our long-term objective is to develop a set of computational tools enabling a multiscale investigation of the physical basis governing biological processes, like electron or hydrogen transfers. The physicochemical basis of ET reactions can be modeled by the Marcus theory using the adiabatic (eq 23) or the nonadiabatic (eq 24) expressions of the rate constant. The latter is expected to be valid in the perturbative limit, for example, when the electronic coupling between the two diabatic states is weak (a situation that may occur, for example, for large donor to acceptor distances or for symmetry forbidden ET reactions).

$$k_{ET}^{A} = \nu \cdot \exp\left(-\frac{\Delta G^{\neq}}{k_B T}\right) \tag{23}$$

$$k_{ET}^{NA} = \frac{2\pi}{\hbar}\frac{1}{\sqrt{4\pi\lambda k_B T}}|H_{12}|^2 \exp\left(-\frac{\Delta G^{\neq}}{k_B T}\right) \tag{24}$$

In these expressions ν is the effective frequency of the system along the reaction coordinate and $\Delta G^{\neq}$ is the Gibbs free energy of activation. Previous studies have shown the efficiency of constrained DFT approaches to evaluate the energetic required to evaluate such rate constants. Here we will alternatively focus on the terms involved in the mixed quantum−classical approach we recently proposed (eq 25).[34] This new rate constant expression has the advantage to cover either the adiabatic, nonadiabatic, or intermediate regimes.[34] This expression was obtained by taking into account the role of quantum decoherence between the two diabatic states characterizing the ET process in the determination of the hopping probability. The reader is referred to ref 34 for a detailed description of our approach. We mention that eq 25 has been derived under the Condon approximations and is expected to be valid when decoherence occurs faster than the typical vibrational frequency of the nuclei participating to the ET reaction coordinate.

$$k_{ET}^{MQC} = \nu \cdot \frac{8\mu^2}{\hbar^2 + 8\mu^2}\exp\left(-\frac{\Delta G^{\neq}}{k_B T}\right); \quad \mu = H_{12}\tau_{dec} \tag{25}$$

The parameter μ is the product of the electronic coupling between the two nonadiabatic electronic states involved in the reaction and a characteristic decoherence time of the system. This latter parameter reflects the time it takes for the nuclei to behave like classical particles.[34] The precise definition of decoherence times for concrete physicochemical problems is still a matter of intense research.[35] Estimation of decoherence times from atomistic simulations is not a straightforward task, and various schemes have been proposed to this end.[36−38]

In a previous paper we estimated τ_{dec} in the short time approximation using Born−Oppenheimer MD simulations in gas phase in the case of a spin-forbidden reaction relevant to the question of dioxygen activation by cuprous complexes.[34] Here we illustrate the capabilities of our hybrid cDFT/MD implementation to estimate both the characteristic decoherence time and the average electronic coupling in the case of ET. The computational protocol was inspired by the work of Prezhdo et al.[39] and later by Lockwood et al.[40] who attributed the major source of decoherence to the loss of overlap between nuclear wave packets evolving on different electronic states. In the short time approximation and in the high-temperature limit, the characteristic decoherence times can be evaluated with eq 26:[39]

$$\tau_{dec} = \left[\left\langle \sum_n \frac{2}{2a_n\hbar^2}(F_{1n} - F_{2n})^2 \right\rangle_T\right]^{-1/2} \tag{26}$$

where n denotes the n^{th} nuclear degree of freedom of associated to a frozen Gaussian wavepacket (FGW) of width a_n and F_{1n} and F_{2n} are the forces acting on the n^{th} degree of freedom, respectively, on the initial and final electronic states. The brackets denote averaging out the temperature T. We draw the attention that eq 26 involves important assumptions and does not cover all

the physics lying behind the term decoherence. A complete description of decoherence effects would require much more complex simulation algorithms that work on the quantum density matrix (see for instance ref 35). Such developments are not the scope of the present paper. Nevertheless eq 26 already provides a valuable mean to estimate the decays of the FC factors for ET reactions from ab initio MD simulations. Skourtis et al. discussed the importance of this term for the detection of non-Condon effects in ET processes.[41] Thus even if eq 26 does not take account of all the physical events leading to decoherence, it remains of primary importance to develop computational tools to reliably evaluate the FC factors. MD simulation using classical force fields has been used to evaluate eq 26 in blue copper proteins.[42,43] However the accuracy of classical force fields may be questionable to estimate such fine effects, especially if metallic centers are concerned. Here we show that cDFT can be used to estimate the FC decay factors from ab initio MD simulations.

In the model presented here, we consider the ET between two lithium ions across a polypeptide chain of increasing length n. To investigate the effect of the environment on τ_{dec} and H_{12}, we performed these calculations both in the gas phase and with inclusion of explicit water through the use of a hybrid DFT/MM scheme.

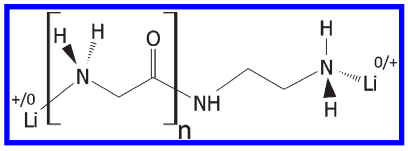

To combine the cDFT calculation performed in deMon2k with the MM calculation performed using the CHARMM package[44] within a QM/MM approach, we use the Cuby framework that interfaces both programs and combines the potentials using a subtractive QM/MM scheme (analogous to the ONIOMM approach)[45] with mechanical embedding of the quantum region. On the resulting potential, Cuby performs MD simulation. Applications of the Cuby framework to both QM/MM calculations[46] and MD simulations using QM-calculated potential[47,48] had been demonstrated earlier; here we merge both approaches for the first time. For the cDFT part the PBE functional[28] was employed with a relativistic effective core potentials (RECP) technique for the heavy atoms, while the DZVP-GGA basis set was used for hydrogen atoms. We have used the Hirshfeld population analysis with DFT atomic densities to define the cDFT weight matrix elements. The electronic couplings are computed according the prescriptions of Wu and Van Voorhis.[49] The classical subsystem only contains flexible SPC water molecules[50] and one chloride counterion. The volume of the box is $60 \times 60 \times 60$ Å^3. The use of flexible water model in this study has two reasons: First, it covers vibrational motions of the solvent molecules that might affect the decoherence time, creating a rapidly fluctuating environment. Second, it makes the formulation of the QM/MM MD more straightforward when no constraints are present. The quantum partition includes the lithium ions and the polypeptide as well as six water molecules surrounding the lithium atoms.

We performed 1.5 ps long MD simulations in the NVT ensemble (at T = 300 K) for each of the five systems in gas phase and within the aqueous environment. The time step was set to 0.5 f, and we used the Nose−Hoover thermostat with a coupling time of 0.1 ps. The simulations were equilibrated for 0.5 ps, and the data for the electronic coupling and decoherence time calculations were accumulated over the remaining 1 ps of simulation. In some cases however multiple simulations were run in parallel to achieve the equalivalent of 1 ps more rapidely. These quantities of interest here are to be computed for molecular configurations associated to degeneracy of the two redox states (the seam). Thus, to sample molecular configurations along the seam, the simulations were biased by application of an harmonic potential E_{bias} on the diabatic energy gap ΔE ($E_{bias} = k_{bias}\Delta E^2$), where k_{bias} was set to 2×10^3 kcal·mol^{-1}/(kcal·mol^{-1})^2. The position of the terminal amine groups and the water molecules is first optimized (by a low-temperature MD simulation) to reach a molecular configuration associated to degeneracy of the diabatic states. Then, the lithiums, the terminal amine groups, and the water molecules were fixed in space during the simulations in order to control the donor to acceptor distance. These geometrical restrains may artificially increase decoherence times, since the local motions around the donor and acceptor groups are partially frozen. However our objectives in the present study are to illustrate the technical feasibility of cDFT/MM MD simulations with deMon2k and to investigate the effects of the bridge length on H_{DA} and τ_{dec}. We thus expect that the trends obtained with the present protocol remains valid for fully relaxed geometries. The statistical analysis of the MD simulations outputs were realized with the R Project for Statistical Computing[51] and the coda package.[52]

The dependence of the average electronic coupling term on the chain length is given in Figure 3. In gas phase, the coupling values range from ca. 15 cm^{-1} for a distance of 10.5 Å to 10^{-2} cm^{-1} for larger distances (24 Å). The latter match well those found by others on related systems with alternative methods, like the tunneling current approach.[53] As expected, an exponential decay of the electronic coupling with the distance is obtained with a decay factor of -0.52 ± 0.02 Å^{-1}. In a nonadiabatic regime, this value would lead to a decay for the rate constant of around -1.04 Å^{-1}, in excellent agreement with the experimental value (-1.1 Å^{-1}) reported by Lenden et al. for the ET transfer decay rate through β-strands.[54] Similar values are obtained when an aqueous environment is included in the simulations with a characteristic decay factor of -0.58 ± 0.01 Å^{-1}.

Previous papers have reported the fluctuations of the electronic coupling for ET in the diabatic regimes for the QTTFQ molecule[27] or for static long range ET.[55] However, this study is to our knowledge the first application of the cDFT technique to the computation of MD-averaged electronic couplings on a wide range of donor−acceptor distances. Additionally, we have improved it by the application of a harmonic potential constraining in the cDFT calculations which enforces sampling of the seam region. This is possible only because quantum mechanical calculation is used to obtain the potential, in contrast to previous studies using MM. Such a quantum approach allows going beyond our previous simulation protocols to evaluate the fluctuations of the coupling elements from pure classical MD simulations.[56,57]

The FC decay times as computed with eq 26 are reported in Table 4 for two values of the nuclear wave packets width. One is the high-temperature (HT) values (a_n^{HT}) proposed in ref 58, while the others are the ab initio based values (Møller−Plesset with second-order corrections, a_n^{MP2}) proposed by Thompson et al.[59] In gas phase, the decoherence time is around 5.3 fs for the MP2 widths and 6.8 fs for the HT widths. Remarkably we find that these results are not sensitive to the length of the polypeptide chain. These findings can be understood by looking at eq 26.

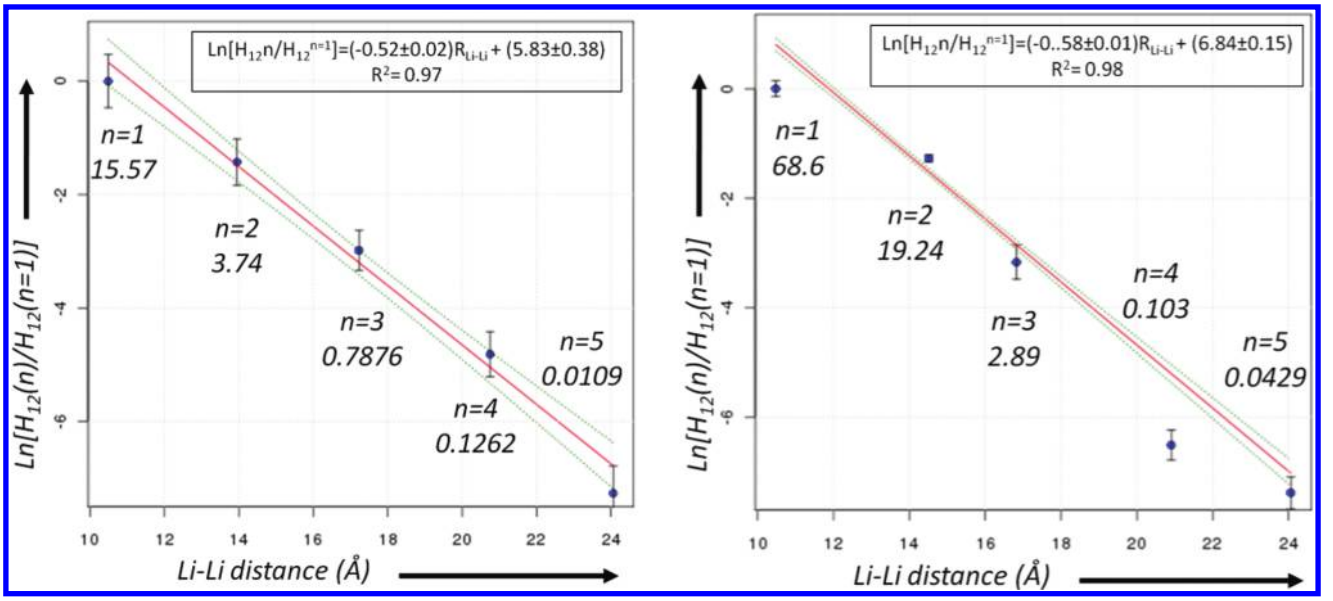

Figure 3. Linear decay of the logarithm of the average electronic coupling for a peptide-mediated ET between a lithium atom and its cationic form either in gas phase (left) or in water (right). The electronic coupling terms for each bridge length (n) are given in cm^{-1}. The associated uncertainties correspond to a confidence interval of 95%. The red curves are the linear regressions on the average points taking account their uncertainties. The green dashed curves are obtained from the linear models with a confidence interval of 95%.

Table 4. Decay Times of the HT FC Factors for Different Donor−Acceptor Distances[a]

		GP τ_{dec}			solv. τ_{dec}	
n	R_{Li-Li}	a_n^{HT}	a_n^{MP2}	R_{Li-Li}	a_n^{HT}	a_n^{MP2}
1	10.5	5.50 ± 0.11	4.16 ± 0.08	10.5	1.55 ± 0.13	1.36 ± 0.29
2	14.0	5.81 ± 0.22	4.27 ± 0.17	14.5	1.93 ± 0.07	1.64 ± 0.05
3	17.2	6.35 ± 0.39	4.59 ± 0.21	16.8	1.82 ± 0.06	1.56 ± 0.07
4	20.8	6.22 ± 0.30	4.54 ± 0.20	20.9	1.73 ± 0.02	1.50 ± 0.02
5	24.1	6.04 ± 0.18	4.55 ± 0.11	24.1	1.78 ± 0.14	1.53 ± 0.12

[a] HT FC factors (characteristic decoherence time) in fs computed with eq 26 in gas phase (GP) and in water (solv.) and donor−acceptor distances in Å. The uncertainties correspond to a confidence interval of 95%

Indeed the decoherence time as computed with this HT formula depends on one side on the difference in forces applied to each nuclear degree of freedom between the two electronic states and on the other side on the fluctuations of this difference due to the thermal motion of the bridge and environment atoms. The degrees of freedom that contribute the most to decoherence are those who feel the most different forces on the two electronic states. One should thus expect the redox cofactor atoms to be the main contributors to decoherence (here the Li and terminal N atoms), while the contribution of the remote atoms should decrease as these atoms become further away from one of the redox centers. It flows that when increasing the length of the peptide, the supplementary atoms contribute less and less to decoherence. On the other hand, the inclusion of the aqueous environment induces a reduction of the decoherence times by a factor of about one-third. This result is easy to understand since in QM/MM BOMB, many more atoms can impact the motion of the atoms surrounding the redox cofactors compared to gas phase simulations. The FC factors are thus expected to decay more rapidly. It must be also recalled that within the ONIOMM type QM/MM protocol used here, the MM water molecules do not feel by construction different forces on the two electronic states. The influence of the environment when computing eq 26 only appears indirectly through the QM atoms. The realization of so-called diverging trajectories on the two electronic states, as done in ref 34, would be needed to improve the treatment of environmental effects to compute the decay of the FC factors. In addition, the redox cofactors were maintained fixed during the BOMD simulations, hence artificially enhancing the decoherence time compared to fully relaxed systems. Nevertheless our simulations confirm that decoherence, as estimated by eq 26, is essentially a local property of the redox cofactors, in contrast to the electronic coupling whose amplitude strongly depends on the bridge length.

CONCLUSIONS

We have described our parallel implementation of the constrained DFT approach in the DFT program deMon2k. Compared to our previous work we have added multiple supplementary population schemes to define the cDFT weight matrices. Additionally, analytical energy gradients have been implemented, enabling geometry optimizations and BOMD simulations at a computational cost similar to regular DFT. Hybrid QM/MM computations are also available either using the CUBY framework as described here as well as with the previously presented CHARMM/deMon2k interface.[60]

We have applied this technique to investigate the fluctuations of the electronic coupling and of the FC factor for a long-range ET (LRET) through a polypeptide chain based on cDFT and cDFT/MM MD simulations. The computed decay of the average electronic coupling through β-strands was found to be in almost perfect agreement with the experimental trends obtained from measurement on Ru-modified proteins. Our results confirm the possibility to parametrize coarse grained models to interpret

biological LRET based on high-level quantum chemistry computation. The decay of the time-dependent FC factor, that can be identified as a possible source of quantum decoherence in biological ET, was shown to be independent of the donor–acceptor distance.

This study demonstrates the efficiency of the implementation of the cDFT approach in deMon2k and opens the door toward the application of this accurate quantum chemistry method to a large variety of biological topics. The deMon2k routines enabling cDFT are available on request. Please contact the authors.

AUTHOR INFORMATION

Corresponding Author

*E-mail: aurelien.de-la-lande@u-psud.fr.

Notes

The authors declare no competing financial interest.

ACKNOWLEDGMENT

The authors wish to thank P. Pernot, F. Cailliez, D. R. Salahub, and A. M. Köster. This work is a part of research project no. Z40550506 of the Institute of Organic Chemistry and Biochemistry, Academy of Sciences of the Czech Republic. The authors thank the European DEISA Consortium for providing computational resources through the DECI program (DFT-DECO project). A.L. wishes to thank University Paris-Sud for special financial support.

REFERENCES

(1) Dederichs, P. H.; Blügle, S.; Zeller, R.; Akai, H. *Phys. Rev. Lett.* **1984**, *53*, 2512.
(2) Wesolowski, T. A.; Warshel, A. *J. Phys. Chem.* **1993**, *97*, 8050.
(3) Hong, G.; Strajbl, M.; Wesolowski, T. A.; Warshel, A *J. Comput. Chem.* **2000**, *21*, 1554.
(4) Wu., Q.; Van Voorhis, T. *Phys. Rev. A* **2005**, *72*, 024502.
(5) Van Voorhis, T.; Kowalczyk, T.; Kaduk, B.; Wang, L.-P.; Cheng, C.-L.; Wu, Q. *Annu. Rev. Phys. Chem.* **2010**, *61*, 149.
(6) Yang, W.; Ayers, P. W.; Wu, Q. *Phys. Rev. Lett.* **2004**, *92*, 146404.
(7) Ogawa, T.; Sumita, M.; Shimodo, Y.; Morihashi, K. *Chem. Phys. Lett.* **2011**, *511*, 219.
(8) Oberhofer, H.; Blumberger, J. *J. Chem. Phys.* **2009**, *131*, 064101.
(9) Rapacioli, M.; Spiegelman, F.; Scemama, A.; Mirtschink, A. *J. Chem. Theory Comput.* **2011**, *7*, 44.
(10) Sena, M. P. A.; Miyazaki, T.; Bowler, D. R. *J. Chem. Theory Comput.* **2011**, *7*, 884.
(11) de la Lande, A.; Salahub, D. R. *J. Mol. Struct. THEOCHEM* **2010**, *943*, 115.
(12) Köster, A. M.; Calaminici, P.; Casida, M. E.; Flores-Moreno, R.; Geudtner, G.; Goursot, A.; Heine, Th.; Ipatov, A.; Janetzko, F.; del Campo, J. M.; Patchkovskii, S.; Reveles, J. U.; Salahub, D. R. Vela, A. *deMon2k*; The deMon Developers: Cinvestav, Mexico City, 2006; http://www.demon-software.com/public_html/index.html.
(13) Köster, A. M.; Reveles, J. U.; del Campo, J. M. *J. Chem. Phys.* **2004**, *121*, 3417.
(14) Köster, A. M.; del Campo, J. M.; Janetzko, F.; Zuniga-Gutierrez, B. *J. Chem. Phys.* **2009**, *130*, 114106.
(15) de la Lande, A.; Salahub, D. R.; Maddaluno, J.; Scemama, A.; Pilme, J.; Parisel, O.; Gérard, H.; Caffarel, M.; Piquemal, J.-P. *J. Comput. Chem.* **2011**, *32*, 1171.
(16) Guerra, C. F.; Handgraaf, J.-W.; Baerends, E. J.; Bickelhaupt, F. M. *J. Comput. Chem.* **2003**, *25*, 189.
(17) Hirshfeld, F. L. *Theor. Chim. Acta* **1977**, *44*, 129.
(18) Wu., Q.; Van Voorhis, T. *J. Chem. Theory Comput.* **2006**, *2*, 765–774.
(19) Krack, M.; Köster, A. M. *J. Chem. Phys.* **1998**, *108*, 3226.
(20) Becke, A. D. *J. Chem. Phys.* **1987**, *88*, 2547.
(21) Stratmann, R. E.; Scuseria, G. E.; Frisch, M. J. *Chem. Phys. Lett.* **1993**, *257*, 213.
(22) Pulay, P. *Mol. Phys.* **1969**, *17*, 197.
(23) Baker, J.; Andzelm, J.; Scheiner, A.; Delley, B. *J. Chem. Phys.* **1994**, *101*, 8894.
(24) Köster, A. M. *J. Chem. Phys.* **2003**, *118*, 9943.
(25) Gautier, N.; Dumur, F.; Lloveras, V.; Vidal-Gancedo, J.; Veciana, J.; Rovira, C.; Hudhomme, P. *Angew. Chem.* **2003**, *115*, 2871.
(26) Wu, Q.; Van Voorhis, T. *J. Phys. Chem. A* **2006**, *110*, 9212.
(27) Oberhofer, H.; Blumberger *J. Chem. Phys.* **2010**, *133*, 244105.
(28) Perdew, J. P.; Burke, K.; Ernzerhof, M. *Phys. Rev. Lett.* **1996**, *77*, 3865.
(29) Köster, A. M.; Flores-Moreno, R.; Reveles, J. U. *J. Chem. Phys.* **2004**, *121*, 681.
(30) Calaminici, P.; Domínguez-Soria, V. D.; Geudtner, G.; Hernández-Marín, E.; Köster, A. M. *Theor. Chem. Acc.* **2006**, *115*, 221.
(31) Geudtner, G.; Janetzko, F.; Köster, A. M.; Vela, A.; Calaminici, P. *J. Comput. Chem.* **2006**, *27*, 483.
(32) Goursot, A.; Mineva, T.; Krishnamurty, S.; Salahub, D. R *Can. J. Chem.* **2009**, *87*, 1261.
(33) Gamboa, G. U.; Calaminici, P.; Geudtner, G.; Köster, A. *J. Phys. Chem. A* **2008**, *112*, 11969.
(34) de la Lande, A.; Řezáč, J.; Lévy, B.; Sanders, B. C.; Salahub, D. R. *J. Am. Chem. Soc.* **2011**, *133*, 3883.
(35) Kapral, R. *Annu. Rev. Phys. Chem.* **2006**, *57*, 129.
(36) Granucci, G.; Persico, M.; Zoccante, A. *J. Chem. Phys.* **2010**, *126*, 134111.
(37) Shenvi, N.; Subotnik, J. E.; Yang, W. *J. Chem. Phys.* **2011**, *134*, 144102.
(38) Cheng, S. C.; Zhu, C.; Liang, K. K.; Lin, S. H.; Truhlar, D. G. *J. Chem. Phys.* **2008**, *129*, 024112.
(39) Prezhdo, O. V.; Rossky, P. J. *J. Chem. Phys.* **1997**, *107*, 5863.
(40) Lockwood, D. M.; Cheng, Y.-K.; Rossky, P. J. *Chem. Phys. Lett.* **2001**, *345*, 159.
(41) Skourtis, S. S.; Balabin, I. A.; Kawatsu, T.; Beratan, D. N *Proc. Natl. Acad. Soc. U.S.A.* **2005**, *102*, 3552–3557.
(42) Lockwood, M.; Cheng, Y.-K.; Rossky, P. J. *Chem. Phys. Lett.* **2001**, *345*, 159.
(43) Lockwood, D. M.; Hwang, H.; Rossky, P. J. *Chem. Phys.* **2001**, *268*, 285.
(44) Brooks, B. R.; et al. *J. Comput. Chem.* **1983**, *4*, 187.
(45) Dapprich, S.; Komáromi, I.; Suzie Byun., K.; Morokuma, K.; Frisch, M. J. *J. Mol. Struct. THEOCHEM* **1999**, *461*, 121.
(46) Fanfrlík, J.; Brynda, J.; Řezáč, J.; Hobza, P.; Lepšík, M. *J. Phys. Chem. B* **2008**, *112*, 15094.
(47) Řezáč, J.; Hobza, P *J. Chem. Theory Comput.* **2008**, *4*, 1835.
(48) Valdes, H.; Spiwok, V.; Rezac, J.; Reha, D.; Abo-Riziq, A. G.; de Vries, M. S.; Hobza, P. *Chem.—Eur. J.* **2008**, *14*, 4886.
(49) Wu., Q.; Van Voorhis, T. *J. Chem. Phys.* **2006**, *125*, 164105.
(50) Wu, Y.; Tepper, H. L.; Voth, G. A. *J. Chem. Phys.* **2006**, *124*, 024503.
(51) Bates, D.; Chambers, J. et al. *The R Project for Statistical Computing*; Statistics Department, University of Auckland: Auckland, New Zealand, 2011; http://www.r-project.org/
(52) Plummer, N.; Best, N.; Cowles, K.; Vines, K. *Output analysis and diagnostics for MCMC*, version 0.14-6, 2011.
(53) Daizadeh, I.; Guo, J. -X.; Stuchebrukhov, A. A. *J. Chem. Phys.* **1999**, *110*, 8865.
(54) Langen, R.; Chang, I.-Y.; Germanas, J. P.; Richards, J. H.; Winkler, J. R.; Gray, H. B. *Science* **1995**, *268*, 1733.
(55) Ding, F.; Wang, Haobin.; Wu, Q.; Van Voohris, T.; Chen, S.; Konopelski, J. P. *J. Phys. Chem. A* **2010**, *114*, 6039.
(56) de la Lande, A.; Martí, S.; Parisel, O.; Moliner, V. *J. Am. Chem. Soc.* **2007**, *129*, 11700.

(57) de la Lande, A.; Babcock, N.; Řezáč, J.; Sanders, B. C.; Salahub, D. R. *Proc. Natl. Acad. Soc. U.S.A.* **2010**, *107*, 11799.
(58) Neria, E.; Nitzan, A. *J. Chem. Phys.* **1993**, *99*, 1109.
(59) Thompson, A. L.; Punwong, C.; Martínez, T. J. *Chem. Phys.* **2010**, *370*, 70.
(60) Lev, B.; Zhang, R.; de la Lande, A.; Salahub, D. R.; Noskov, S. Y. *J. Comput. Chem.* **2010**, *31*, 1015–1023.